



UNIVERSITY OF LEEDS

This is a repository copy of *Reaction Rate Governs the Viscoelasticity and Nanostructure of Folded Protein Hydrogels*.

White Rose Research Online URL for this paper:

<https://eprints.whiterose.ac.uk/166634/>

Version: Accepted Version

---

**Article:**

Aufderhorst-Roberts, A [orcid.org/0000-0003-3559-9423](https://orcid.org/0000-0003-3559-9423), Hughes, M, Hare, A et al. (4 more authors) (2020) Reaction Rate Governs the Viscoelasticity and Nanostructure of Folded Protein Hydrogels. *Biomacromolecules*, 21 (10). [acs.biomac.0c01044](https://doi.org/10.1021/acs.biomac.0c01044). pp. 4253-4260. ISSN 1525-7797

<https://doi.org/10.1021/acs.biomac.0c01044>

---

© 2020 American Chemical Society. This is an author produced version of an article published in *Biomacromolecules*. Uploaded in accordance with the publisher's self-archiving policy.

**Reuse**

Items deposited in White Rose Research Online are protected by copyright, with all rights reserved unless indicated otherwise. They may be downloaded and/or printed for private study, or other acts as permitted by national copyright laws. The publisher or other rights holders may allow further reproduction and re-use of the full text version. This is indicated by the licence information on the White Rose Research Online record for the item.

**Takedown**

If you consider content in White Rose Research Online to be in breach of UK law, please notify us by emailing [eprints@whiterose.ac.uk](mailto:eprints@whiterose.ac.uk) including the URL of the record and the reason for the withdrawal request.



[eprints@whiterose.ac.uk](mailto:eprints@whiterose.ac.uk)  
<https://eprints.whiterose.ac.uk/>

# Reaction Rate Governs the Viscoelasticity and Nanostructure of Folded Protein Hydrogels

Anders Aufderhorst-Roberts,<sup>†</sup> Matt D.G. Hughes,<sup>†</sup> Andrew Hare,<sup>†</sup> David A. Head,<sup>‡</sup> Nikil Kapur,<sup>¶</sup> David J. Brockwell,<sup>§</sup> and Lorna Dougan<sup>\*,†</sup>

<sup>†</sup>*School of Physics and Astronomy, University of Leeds, Leeds, UK*

<sup>‡</sup>*School of Computing, University of Leeds, Leeds, UK*

<sup>¶</sup>*School of Mechanical Engineering, University of Leeds, Leeds, UK*

<sup>§</sup>*School of Molecular and Cellular Biology, University of Leeds, Leeds, UK*

E-mail: L.Dougan@leeds.ac.uk

## Abstract

Hydrogels constructed from folded protein domains are of increasing interest as resilient and responsive biomaterials, but their optimisation for applications requires time-consuming and costly molecular design. Here, we explore a complementary approach to control their properties by examining the influence of crosslinking rate on the structure and viscoelastic response of a model hydrogel constructed from photochemically crosslinked bovine serum albumin (BSA). Gelation is observed to follow a heterogeneous nucleation pathway in which BSA monomers crosslink into compact nuclei that grow into fractal percolated networks. Both the viscoelastic response probed by shear rheology and the nanostructure probed by small angle x-ray scattering (SAXS) is shown to depend on the photochemical crosslinking reaction rate, with increased reaction rates corresponding to higher viscoelastic moduli, lower fractal dimension and higher fractal cluster size. Reaction rate dependent changes are shown to be consistent

with a transition between diffusion- and rate- limited assembly and the corresponding changes to viscoelastic response are proposed to arise from the presence of non-fractal depletion regions, as confirmed by SAXS. This controllable nanostructure and viscoelasticity constitutes a potential route for the precise control of hydrogel properties, without the need for molecular modification.

## Introduction

In nature, folded globular proteins carry out a wide variety of functions, that arise from their ability to undergo conformational change under precise chemical and mechanical stimuli. Inspired by this, an emerging body of research has explored the potential of leveraging this function by chemically crosslinking folded proteins into hydrogels.<sup>1</sup> So-called folded protein hydrogels are capable of reproducing a variety of functional properties such as mimicking the nonlinear elastic response of muscles,<sup>2-5</sup> maintaining their mechanical integrity even after large deformations<sup>6,7</sup> or after exposure to chemical reduction<sup>8</sup> and to be mechanically responsive to chemical stimuli.<sup>9</sup> The design of these hydrogels depends on translating the precise molecular scale mechanical response of the individual proteins, into bulk mechanical properties<sup>10</sup> through recombinant design.<sup>11,12</sup> While such approaches have been shown to be both precise and effective in creating folded proteins with desired mechanical properties, they have a number of limitations. Both the recombinant design and the subsequent expression and purification of the protein typically require significant optimisation. Furthermore, the key advantage of folded hydrogels is their highly precise mechanical response.<sup>13</sup> But this advantage presents an immediate challenge: how can the precise mechanical response of a single protein in a hydrogel be tuned without extensive biomolecular design?

In this work we address this challenge by exploring how nanostructure and viscoelastic response can be controlled through the reaction rate of chemical crosslinking. The conventional view in the literature is that hydrogel properties, particularly for polymer gels, are predominantly governed by the extent of the crosslinking reaction<sup>14,15</sup> rather than its rate.

Indeed, photochemical crosslinking approaches have been used to create gradients in hydrogel stiffness by spatially varying the reaction extent.<sup>16–18</sup> However, even without the presence of a spatial gradient, globular particles such as folded proteins are able to form complex hierarchical structures whose architecture can be tuned by balancing the crosslinking rate and the particle diffusion rate.<sup>19–21</sup> Similar principles govern the aggregation of proteins in nature, where small changes in reaction rate have been shown to result in striking changes to globular protein fibrillization.<sup>22–24</sup>

To explore how these principles can be applied to folded protein hydrogel systems, we construct hydrogels from the model folded protein, bovine serum albumin (BSA). We photochemically crosslink BSA via the commonly used  $[\text{Ru}(\text{bpy})_3]^{2+}$  strategy,<sup>25</sup> by which the protein’s surface exposed aromatic residues<sup>26</sup> are radicalised and subsequently converted into a permanent covalent bonds. While the suitability of ruthenium crosslinking for biological applications remains a matter of debate,<sup>27</sup> due to concerns about toxicity, it remains an excellent model approach due to its specificity and high yield. The reaction rate is varied by adjusting the intensity of illumination, using a custom built device to trigger crosslinking in situ (figure ??), with the reaction rate being controlled externally through modifying the illumination intensity. The high resilience of BSA to unfolding and the permanent nature of the dityrosine bonds makes this an attractive model “chemical gel” system. Unlike colloidal gels, whose assembly appears to be governed by glassy dynamics,<sup>28</sup> chemical gels are well characterised by percolation theory<sup>29</sup> which predict a gelation process that is governed by the nucleation, growth and connection of fractal clusters.<sup>30</sup> This has motivated numerous rheological studies of the evolving viscoelasticity of the gel during percolation and its relationship to parameters such as the fractal dimension of the underlying clusters<sup>31</sup>, the degree of mixing in multicomponent gels<sup>32</sup> and the kinetics of chemical crosslinking.<sup>33</sup> An underlying assumption of the percolation model is that the viscoelastic response is directly governed by the fractal dimension of percolated clusters.<sup>34</sup>

Here, we use the percolation model of gelation to quantify the final viscoelastic response

hydrogels using oscillatory rheology. The oscillatory rheological time sweeps are analysed with a simple kinetic model,<sup>35,36</sup> which quantifies the growth kinetics of the hydrogel network from their initial nuclei. This allows us to quantify the critical size of the assembled BSA nuclei, above which crosslinking accelerates, leading to network percolation. The final mechanical and structural properties of the gel are then analysed in relation to their fractal dimension by drawing on models of reaction- and diffusion-limited assembly.<sup>37,38</sup> Briefly, these models predict a well-defined relationship between reaction rate and structure such that at sufficiently high reaction rates, the assembly is said to be diffusion limited and the critical nuclei coarsen into clusters of low fractal dimension. In the opposite limit of low reaction rates, the process is termed reaction rate limited and the resulting structures are denser with a higher fractal dimension. This framework and its variants were originally conceived to explain colloidal assembly but have since been applied to a wide variety of different systems, including colloid polymer mixtures,<sup>39</sup> dynamically growing particles,<sup>40</sup> colloidal gels,<sup>20,41</sup> nanorods<sup>42</sup> and aerogels.<sup>43</sup> We confirm the validity of this framework for folded protein hydrogels by quantifying the structural parameters through SAXS and correlate these results with the hydrogels' rheological behaviour to derive a simple model for the relation between kinetics, viscoelastic response and structure.

## Experimental

### Hydrogel Preparation

Bovine serum albumin (BSA) hydrogels are prepared as follows. BSA protein was suspended in 25 mM sodium phosphate, pH = 7.4 and centrifuged for 1 minute at 5000 RCF, retaining the supernatant to ensure that all insoluble protein was removed. Protein concentration was measured by absorption at 280nm, using an extinction coefficient of  $43824\text{M}^{-1}\text{cm}^{-1}$ , and diluted to 10-100 mg/ml, corresponding to volume fractions  $\phi$  of between 0.007-0.075, given BSA's molecular weight of 66.5 kDa and assuming a physical volume of BSA of  $82.4\text{nm}^3$ <sup>44</sup>

Tris(2,2'-bipyridyl)-dichlororuthenium(II) hexahydrate ( $\text{Ru}(\text{BiPy})_3$ ) and sodium persulfate (NaPS) were added to the sample directly before use, with final concentrations  $100\mu\text{M}$   $\text{Ru}(\text{BiPy})_3$  and 50 mM NaPS.

Sample gelation was initiated by 1 hour of in-situ illumination with a 460nm light emitting diode. This timescale is in excess of the typical timescale used for ruthenium-APS mediated crosslinking (of order 10s of seconds<sup>45</sup>). Together with the high stoichiometric excess of the NaPS crosslink initiator over the protein, this long timescale was chosen to ensure that all monomeric BSA would be converted over the course of the experiment, irrespective of the illumination intensity used. Intensity was calibrated at 452nm, the maximum absorbance wavelength of  $\text{Ru}(\text{BiPy})_3$ ,<sup>25</sup> using a PM100D power meter equipped with a S470C thermal sensor and adjusted within the range  $5\text{-}40\text{mW}\cdot\text{cm}^{-2}$  by controlling the input current and using a series of 1.6mm polyvinyl chloride filters.

## Shear Rheology

Rheology measurements were performed using a stress-controlled rheometer (Kinexus Malvern Pro) equipped with a 20mm steel plate and plate geometry. A custom device (figure ?? ) was built for in-situ illumination during shear rheology. Low viscosity (5 ctSt) mineral oil was applied to the air-sample interface to prevent evaporation and the measurements were performed at room temperature. The linear viscoelastic moduli  $G'$  and  $G''$  were probed at a frequency of 0.5Hz and a shear strain amplitude of 1%. The transient response of the hydrogels was quantified by a creep test, in which the sample strain was probed at a constant shear stress of 1kPa, corresponds to the linear viscoelastic region for all hydrogels in this study.

## Circular Dichroism

Circular dichroism (CD) measurements were performed on an Applied Photophysics Chirascan CD spectropolarimeter with a 0.001cm path length quartz cuvette, averaging measure-

ments over 1s.

## Small angle X-Ray Scattering (SAXS)

SAXS measurements were performed using 1mm path length borosilicate glass capillary tubes. For BSA solutions, a Anton Parr SAXSpace system (q-range of  $0.01\text{\AA}^{-1} - 0.7\text{\AA}^{-1}$ ) was used while measurements on BSA hydrogels were conducted in the Materials Characterisation Laboratory of the ISIS Spallation Source, on the Nano-inXider SAXS equipment (working q-range of  $0.0044\text{\AA}^{-1} - 0.4\text{\AA}^{-1}$ ). All scattering curve fitting was carried out using Sasview. Scattering curves of BSA suspensions before gelation were fitted with an ellipsoidal form factor and a Hayter-MSA electrostatic repulsion structure factor. This allows the ellipsoidal major and minor radii of the scattering object to be extracted. Scattering curves of hydrogel samples were fitted using the following fractal structure model, as developed in our previous work:<sup>46</sup>

$$I(Q) = V\phi\Delta\rho^2[(1 - f_c)P(Q) + f_cP(Q)S(Q)] + I_0 \quad (1)$$

Here V is the physical volume of the BSA monomers,  $\Delta\rho$  is the difference in scattering length density between the protein and solvent, P(Q) is the ellipsoidal monomer form factor derived from scattering measurements of BSA under dilute conditions (figure ?? (b)) and  $I_0$  is the background intensity. The free variables in this fitting model are the fractions of protein in fractal clusters  $f_c$  and the fractal structure factor S(Q), defined as:<sup>47</sup>

$$S(Q) = \frac{D_f \cdot \Gamma(D_f - 1) \cdot \sin[(D_f - 1)\tan^{-1}(Q\xi)]}{[1 + (Q\xi)^{-2}]^{\frac{D_f - 1}{2}} \cdot (Q \cdot R_0)^{D_f}} \quad (2)$$

Where the free parameters  $D_f$  and  $\xi$  are mass fractal dimension and the correlation length respectively.  $R_0$  is minimum fractal length scale, which we define as the monomer radius of BSA.

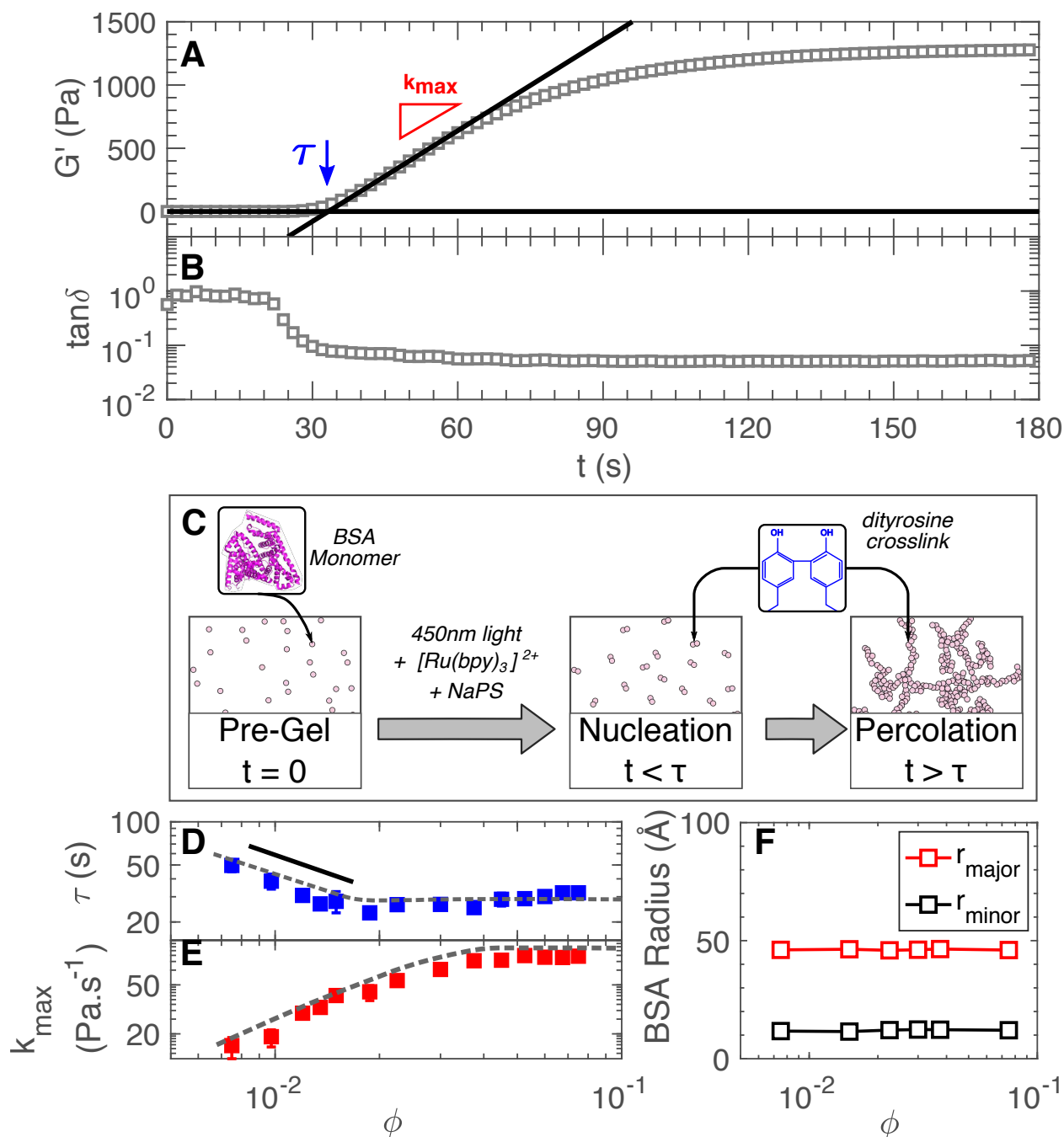


Figure 1: Representative rheology time sweep of BSA hydrogel (volume fraction  $\phi = 0.019$ ) during gelation as quantified by  $G'$ ,  $G''$  (a) and  $\tan \delta$  (b). Gelation is consistent with a model of heterogeneous nucleation (c), with kinetic parameters  $\tau$  (d) and  $k_{max}$  (e) that scale with  $\phi$  as approximately unitary power law fits (solid line). Dashed lines are guides for the eye. SAXS analysis of pre-gel suspensions, using an ellipsoidal form factor reveals no change in the elliptical minor or major radii, precluding the possibility of aggregates forming at high  $\phi$  (f)

# Results and Discussion

We first examine the time dependent viscoelastic response of BSA with respect to crosslinking time for  $\phi = 0.019$  as shown in figure 1. Initially,  $\tan\delta = G''/G' \approx 1$ , indicating a viscoelastic fluid. At a later time  $\tau$ ,  $G'$  and  $G''$  increase while  $\tan\delta$  decreases sharply. We regard this crossover from viscous to elastic behaviour as being indicative of the formation of a percolated hydrogel network.<sup>29,48</sup>  $G'$  reaches a maximum rate of increase  $k_{max}$  at the point of inflection and approaches a steady state within the observation window for  $t < 180s$  for all  $\phi$  (figure ??).

We assess the kinetic parameters of gel formation using nucleated polymerisation theory,<sup>35,49-51</sup> which models the prolonged lag phase  $\tau$  as a heterogeneous nucleation process, (figure 1 (c)). Here, the monomers initially form primary nuclei comprising  $n_c$  monomers that lower the energy barrier to subsequent growth, thereby accelerating the rate of crosslinking. This model is broadly applicable to different polymerised structures including gels<sup>35</sup> and we consider it to be appropriate for our rheology data for a number of reasons. Firstly, its applicability demands that the experimental observable, in our case  $G'$ , increases with the polymerised fraction and reaches an upper threshold when assembly is complete,<sup>52</sup> which is indeed what we observe. Secondly, the model assumes that the association of monomers and nuclei is dominated by only one reaction mechanism,<sup>53</sup> in this case the ruthenium-mediated photochemical crosslinking.

Two key kinetic parameters arise from this model. The first of these is the timescale of the lag phase  $\tau$ , which reflects the time taken for secondary growth to dominate over primary nucleation. The second parameter is the peak rate of modulus growth  $k_{max}$ , which is related to the rate of secondary growth. One consequence of this model is that  $\tau$  scales with  $\phi$  through a power law function. To test this we identify  $k_{max}$  by applying a numerical derivative to the time sweep data and use the common method of defining  $\tau$  as the intercept of the resulting slope with the x-axis as shown in figure 1(a). We indeed find power law scaling between  $\tau$  and  $\phi$ , for  $\phi < 0.018$ , with a least squares logarithmic fit yielding a power

law exponent of  $0.84 \pm 0.09$ . The value of this exponent allows us to make a number of inferences about the nucleation mechanism. Specifically an exponent greater than 1 would indicate that the lag phase arises from slow primary nucleation,<sup>54</sup> while an exponent of 0.5<sup>55</sup> would instead imply that the lag phase arises from slow secondary growth. Since the observed exponent lies between these regimes, we conclude that both primary nucleation and secondary growth occur at similar rates. Furthermore, the power law exponent is predicted to be equal to  $n_c/2$ ,<sup>56,57</sup> where  $n_c$  denotes the size of the primary nucleus in monomers. This suggests that the critical nuclei comprise an average of  $n_c = 1.68 \pm 0.18$  monomers and that these relatively compact nuclei subsequently undergo secondary growth to form a percolated network at time  $\tau$ .

At higher  $\phi$ , the value of  $k_{max}$  reaches a plateau (figure 1 (e)) and a breakdown of power law scaling between  $\phi$  and  $\tau$  is observed (figure 1 (d)), suggesting a competition between different molecular mechanisms.<sup>54</sup> The most obvious cause for such a transition is that the primary nucleation pathway has a higher concentration dependence than the secondary growth pathway.<sup>35</sup> To verify that this is indeed the case, and not a consequence of concentration dependent phenomena such as protein aggregation,<sup>58</sup> SAXS measurements were performed on concentrated BSA solutions (figure ??). As expected for non-aggregating systems, the resulting fits confirm that the scattering object dimensions remain constant with  $\phi$ , (figure 1 (f)) eliminating the possibility of aggregate clusters forming at higher concentrations.

Having modelled the kinetics of gelation, we next examine the sensitivity of these kinetics to reaction rate, as controlled by the illumination intensity. From the time sweeps (figure ??), we find that lowering the reaction rate demonstrably slows the kinetics of crosslinking as shown by the observed increased  $\tau$  and decreased  $k_{max}$  in figure 2(a)-(b). Applying a power law least squares fit, we find linear scaling between  $\tau$  and illumination intensity and inverse linear scaling between  $k_{max}$  and illumination intensity. Less intuitively, we also observe an unambiguous increase in the steady state values of  $G'$  and  $G''$  (figure 2(c)-(d)) as the reaction

rate is increased. Importantly, this increase can not be attributed to monomer denaturation since CD spectra (figure ??) indicate that  $>95\%$  of the BSA remains folded after gelation, irrespective of reaction rate.

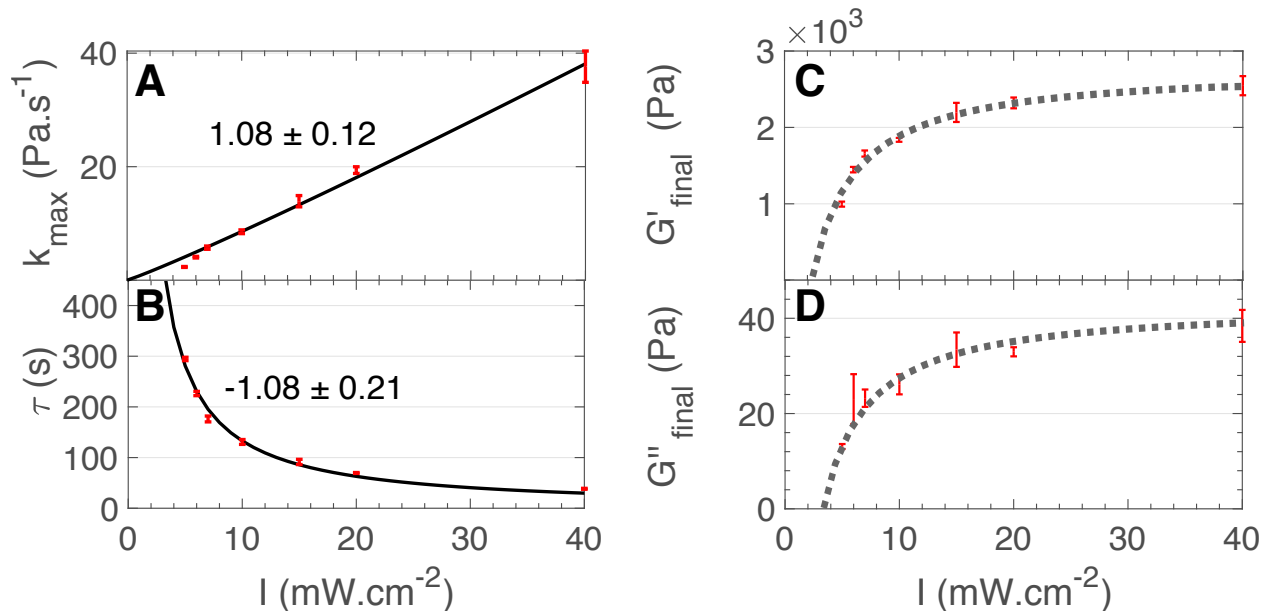


Figure 2: Reaction rate dependence of the kinetic parameters: the maximum rate of modulus growth  $k_{max}$  (a) and the lag time  $\tau$  (b), and of the steady state viscoelastic parameters  $G'$  (c) and  $G''$  (d). Values of  $\tau$  and  $k_{max}$  scale with intensity as approximately unitary power law fits, shown as solid lines. The final steady state values of  $G'$  and  $G''$  increase with increasing intensity. Reaction rate is defined by illumination intensity  $I$  and  $\phi = 0.075$  for all samples. Dashed lines are guides to the eye, error bars represent standard deviation.

To explore the viscoelastic properties further, we probe the transient viscoelastic response, post-gelation at a range of reaction rates for  $\phi = 0.075$ . Frequency spectra (figure 3(a)) show that  $G'$  exceeds  $G''$  over all frequencies and that both  $G'$  and  $G''$  are approximately level, as expected for permanently cross linked networks. We also carry out creep experiments on hydrogels formed at different reaction rates. (figure 3(b)) In agreement with figure 1, slower reaction rates correspond to softer hydrogels as manifested by an increased creep. We examine the mechanistic origins of this creep by fitting the data with so-called Maxwell standard linear solid model. This combines a Maxwell element (spring and dashpot in series) in parallel with a spring element. This constitutive model is inherently reductive but nevertheless provides an excellent fit to the observed creep as shown, in comparison

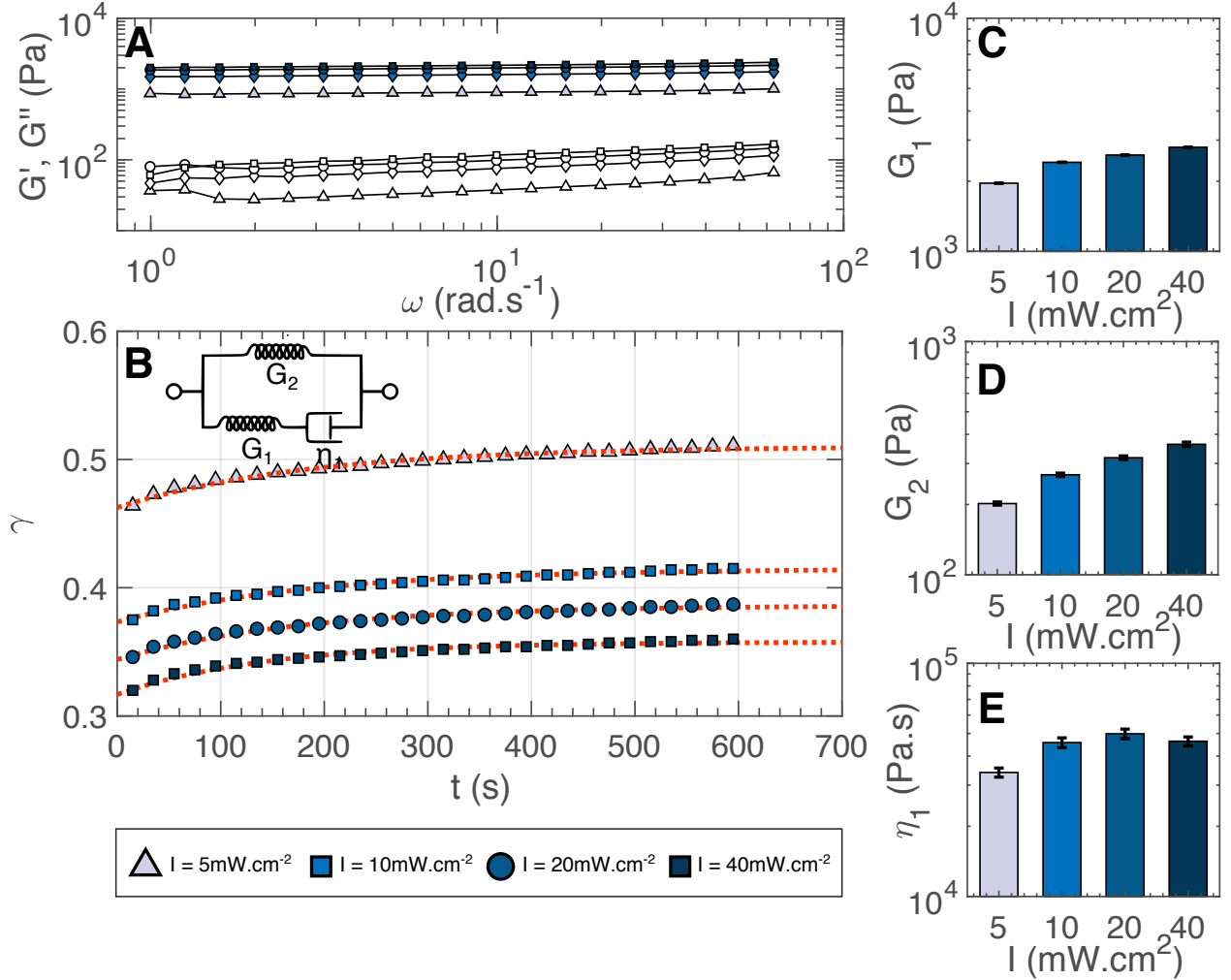


Figure 3: Transient viscoelastic response of BSA hydrogels formed at different reaction rates, as quantified through the illumination intensity  $I$ . For frequency sweeps (a), closed symbols denote  $G'$ , open symbols denote  $G''$ . A weak dependence is observed between  $G'$ ,  $G''$  and angular frequency  $\omega$  and  $G' > G''$  over all frequencies, as expected for permanently cross linked networks. Increasing reaction rate results in increased creep strain (b). A three element standard linear solid model (inset) is fitted, comprising two elastic elements with moduli  $G_1$  and  $G_2$ , and a viscous element with viscosity  $\eta_1$ . The increased creep originates predominantly from a higher value of  $G_1$ , (c) representing the instantaneous elasticity of the network while the entropic elasticity  $G_2$  (d) and viscosity  $\eta_1$  (e) remain relatively unchanged. Error bars are fitting errors.

to other constitutive models, in figure ???. Furthermore the fitted parameters provide phenomenological insights. Specifically, the instantaneous elastic response, which arises from the rotation and lengthening of the chain segments that comprise the percolated network, is represented by the sum of the two springs  $G_1 + G_2$ . The total elastic modulus ( $G_1 + G_2$ ) is

consistently of order  $10^3$ Pa and increases with reaction rate, which validates our approach as it is in good agreement with the oscillatory shear moduli (figure 2(c)-(d)). The quantity  $G_1$  represents the later entropic restoring force that arises from the fluctuation of the network segments and  $\eta_1$  represents the molecular friction from temporary entanglements. The fitted values of the constitutive elements at different reaction rates are shown in figure 3(c)-(e). For all reaction rates,  $G_2$  is approximately an order of magnitude higher than  $G_1$ , suggesting that the network viscoelasticity is predominantly elastic, rather than entropic in origin. Both  $G_1$  and  $G_2$  increase with reaction rate, but do so to different extents:  $G_2$  increases by 80% while  $G_1$  increases by 43%, indicating that the relative entropic and elastic contributions to creep vary with reaction rate. This leads us to propose that the observed differences in viscoelastic response have structural origins and that they arise from differences in the length of the chain segments within the gel network. A possible mechanism for these structural changes would be a transition between so-called rate and diffusion limited assembly mechanisms.<sup>59</sup> Here, when the reaction rate is high, the rate of transport is the only limiting factor to gelation and the process is termed diffusion limited. By contrast, when the reaction rate is low, the reaction rate is instead the limiting factor and the process is termed reaction limited. Diffusion limited assembly typically results in structures with a significantly lower fractal dimension and thus in lower local density of monomers.<sup>37</sup> Decreasing the fractal dimension by increasing the reaction rate would therefore directly correlate to longer segment lengths. This would be consistent with our observation that there is a significant increase in the elastic creep response as the reaction rate is increased.

To test this hypothesis we probe the nanostructure of the BSA hydrogels using SAXS across the previously measured range of reaction rates (figure 4(a)). To extract the quantitative structural parameters we fit the scattering intensity using a fractal structure factor,<sup>47</sup> using an approach that we have previously adopted to fit globular protein hydrogels.<sup>46</sup> Such fractal structures are characteristic to both chemically crosslinked hydrogels<sup>60</sup> and colloidal gels,<sup>61</sup> giving us confidence in our choice of model for our system. A limitation of fractal

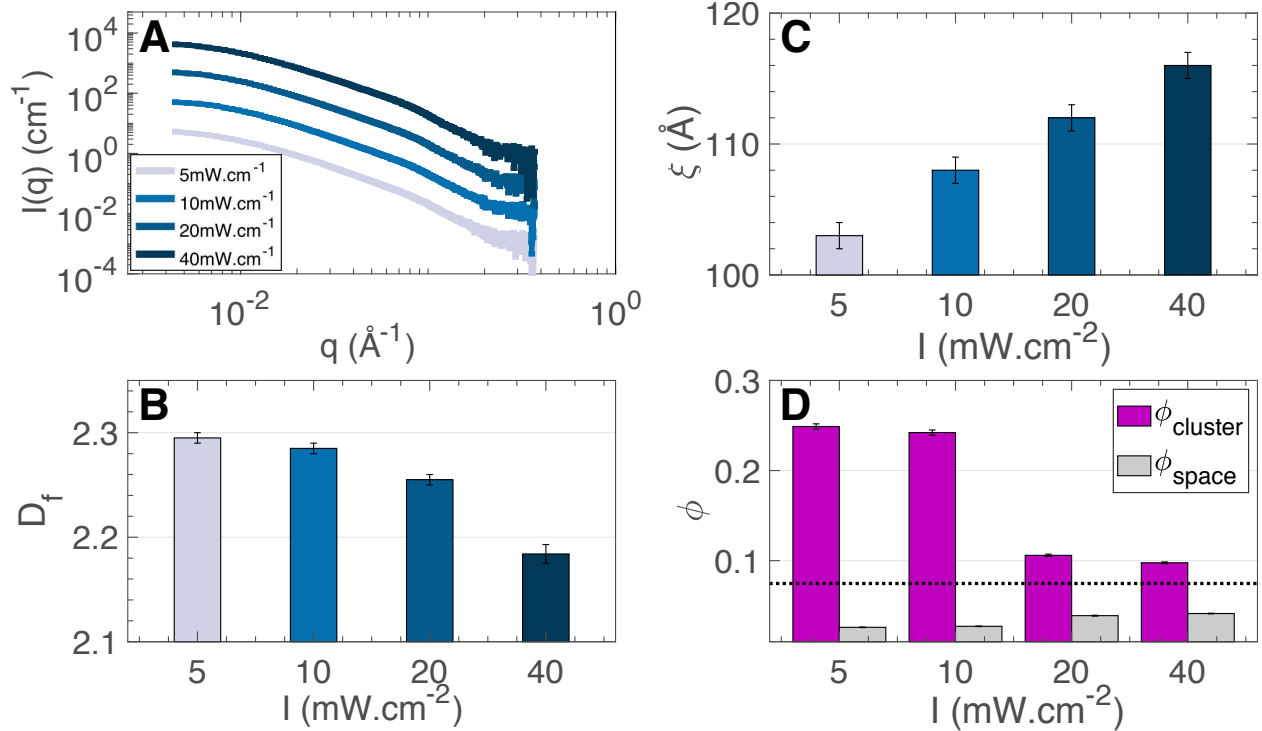


Figure 4: SAXS analysis of hydrogels prepared with variable reaction rates. Plots of scattering intensity (a) are fitted to a fractal model to reveal the fractal dimension  $D_f$  (b) and the characteristic size  $\xi$  (c) of the constituent fractal clusters. Curves are shifted vertically for clarity. Increasing reaction rate by increasing intensity results in a decreased  $D_f$  and an increased  $\xi$ . At higher reaction rates the volume fractions of the fractal clusters  $\phi_c$  and inter-cluster space  $\phi_s$  begin to converge towards the mean volume fraction  $\bar{\phi}$ , indicating increased network uniformity (d). Error bars represent fitting errors.

models when considering clusters that percolate is the possibility of a ‘depletion region’ that surrounds the growing clusters.<sup>20</sup> Accounting for these regions is non-trivial. However, using existing models developed in our group<sup>46</sup> we are able to extract the proportion of monomers that do not exist within fractal clusters, allowing insight into the level of monomer depletion in the inter-cluster space. Further details of this approach are outlined in the supplementary information.

The relevant structural parameters are therefore the proportion of monomers existing within fractal clusters  $f_c$ , the cluster fractal dimension is  $D_f$  and the cluster’s characteristic size is  $\xi$ . The results of these analytical fits (table ??) suggest that, for all reaction rates, a high proportion of monomers ( $\approx 67\%$ ) do indeed exist in fractal clusters. As reaction

rate increases,  $\xi$  is observed to increase (figure 4 (b)) while  $D_f$  appears to decrease (figure 4 (c)). This trend in  $D_f$  is in direct qualitative agreement with simulations of reaction and diffusion limited processes.<sup>62</sup> Furthermore, the measured range of  $D_f = 2.18-2.3$  is consistent with theoretical predictions, which provide an upper limit in three dimensions of  $D_f = 2.5$  for percolated diffusion-limited structures<sup>63</sup> and  $D_f = 3$  for reaction-limited structures.<sup>64</sup>

The data also imply that a significant proportion of monomers exist in non-fractal regions in the inter-cluster spaces during crosslinking. Such depletion regions are usually characterised by a Bragg peak.<sup>20,41</sup> We do not observe such a Bragg peak, which would suggest that if there were any characteristic inter-cluster length scale it exceeds  $1400\text{\AA}$ , the maximum length scale corresponding to the experimental q-range. To investigate this depletion region further, we quantify the volume fractions of the inter-cluster spaces  $\phi_s$  and of the fractal clusters  $\phi_c$ . These variables are extracted by substituting the fitted values of  $D_f$  and  $\xi$  into the radial fractal distribution function as a function of the distance from the cluster centre  $r$ :

$$g(r) = \frac{\rho_k \cdot D_f}{4\pi r_0^{D_f}} r^{D_f-3} e^{-r/\xi} \quad (3)$$

where  $r_0$  is the monomer radius  $2.7\text{nm}$ ,<sup>44</sup>  $\phi$  is protein volume fraction and  $\rho_k$  is the packing density, which we take as  $0.634$ , the packing density of randomly packed spheres. We integrate  $g(r)$  over volume  $V$  to derive the number density  $N(r) = \int \phi g(r) dV$ , giving us the number of monomers in a fractal cluster as a function of radius from the centre of the cluster. From this quantity we find that the radius of the percolating clusters varies from  $140\text{\AA}$  at a an illumination intensity of  $5\text{mW/cm}^2$  to  $195\text{\AA}$  at  $40\text{mW/cm}^2$  (table ??). From the number density it is also possible to calculate  $\phi_c$  and by extension  $\phi_s = 1 - \phi_c$ .

As shown in in figure 4 (d),  $\phi_c$  and  $\phi_s$  converge towards the mean volume fraction of the hydrogel as the reaction rate is increased, indicating an increased network uniformity. Remarkably the associated relative drop in  $\phi_c$  over this range of reaction rates ( $2.55 \pm 0.02$ ) is identical to the relative increase in  $G'$  across the same range ( $2.56 \pm 0.21$ ), suggesting that

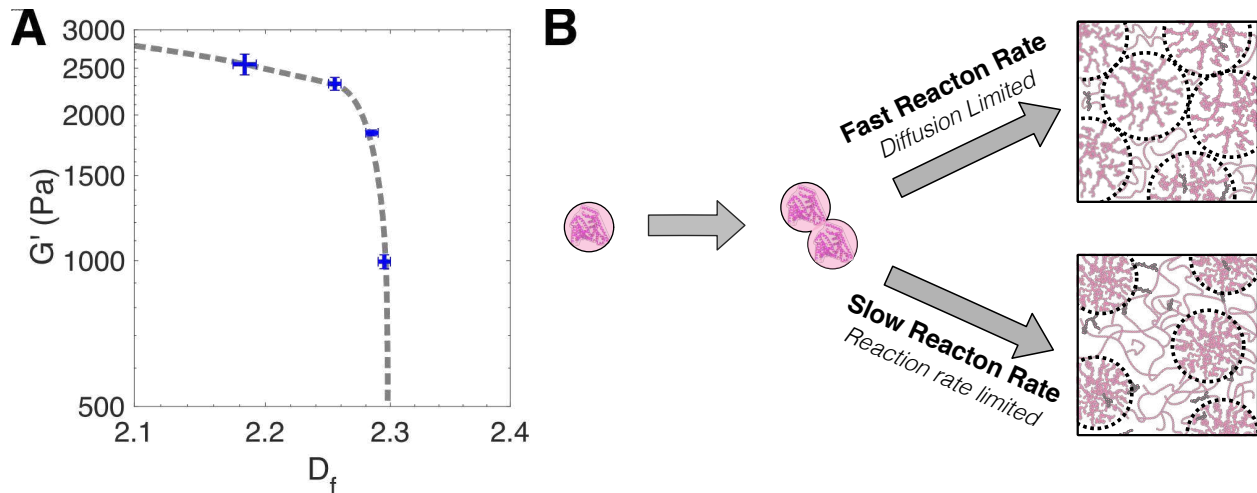


Figure 5: Shear modulus  $G'$  is shown to exhibit strong inverse scaling relation with the fractal dimension  $D_f$ , in contrast with fractal gel theory which predicts  $G'$  to increase exponentially. (a). The source of this discrepancy is proposed to arise from the reaction pathway which transitions from diffusion limited, at fast reaction rates to reaction rate limited at slow reaction rates. (b) In the later case, the clusters are denser and the non-fractal regions contain a lower volume fraction of monomers (figure 4). The resulting network inhomogeneity, as confirmed by scattering data, leads to a decreased shear modulus (figure 2) and an increased creep strain (figure 3). The dashed line is a guide to the eye.

these two independently observed parameters have a common origin.

For ideal fractal gels, the magnitude of the shear modulus is proportional to the proportion of elastically active strands.<sup>65</sup> Because fractal clusters have a scale invariant structure, the number of active strands connecting clusters is independent of cluster size,<sup>66</sup> and leads to the simple relation:  $G' \propto a^{-2}\phi^{2/(3-D_f)}$  where  $a$  denotes the monomer radius,<sup>67</sup> therefore predicting a shear modulus that increases exponentially with  $D_f$ . In stark contrast to this, as depicted in figure 5 (a), the shear modulus is found to strongly decrease with  $D_f$ . Based on this deviation from fractal hydrogel theory, we therefore propose that the elasticity of the network is not governed by the connectivity of fractal clusters but rather by the connectivity of the non-fractal inter-cluster spacing. We rationalise this by considering the distribution of the elasticity across the hydrogel network. For an ideal fractal network, the network is ordered and homogeneous and the elasticity can be described as affine.<sup>68</sup> However, the presence of depletion regions introduces disordered inhomogeneities (figure 4), leading

to a so-called non-affine elasticity that varies locally.<sup>69,70</sup> For non-affine systems, these inhomogeneities are known to be dominant contributors to the shear modulus,<sup>71</sup> relative to the contributions from thermal fluctuations predicted by fractal gel models. This therefore indicates a direct, and previously unidentified, relation between the externally controlled reaction rate, the associated assembly mechanism (diffusion- or rate-limited), the resulting network inhomogeneity and the final viscoelastic response of the crosslinked hydrogel.

## Conclusions

The balance between crosslinking rate and diffusion rate in hydrogel formation has long been known to be a determinant of structural characteristics. In this study we have examined how this phenomenon can influence the viscoelastic response and nanostructure of model folded protein hydrogels constructed from BSA and crosslinked through standard photochemical approaches. We show that the gelation process is characteristic of heterogeneous nucleation, such that monomers in solution associate to form compact ( $n \approx 2$ ) nuclei that grow to form fractal networks. The viscoelastic response of these fractal networks, probed through oscillatory frequency spectra and creep measurements are shown to correlate directly with observed changes in structural parameters. In direct contrast to existing theories of fractal gel mechanics, we observe a decrease in shear modulus and an increase in creep for higher fractal dimension. We propose that this relationship arises from nanoscale network inhomogeneity as revealed by SAXS, specifically due to the presence of non-fractal depletion regions, whose local volume fraction is directly determined by the reaction rate of crosslinking. The decrease in volume fraction within these depletion regions induces an increased structural inhomogeneity, which in turn leads to a reduced shear modulus. Further validation of this proposed mechanism through coarse-grained mesoscale simulations will form the basis of our future work.

The overarching implication of these findings is that there exists a simple relation between

the reaction rate that drives the crosslinking of globular folded proteins and the structure and viscoelastic response of the resulting hydrogels. This is summarised schematically in figure 5 (b). We expect that these principles are, broadly speaking, universally applicable to the emerging field of folded protein hydrogel design. Even within the narrow range of reaction rates reported here ( $5\text{-}40\text{mW}\cdot\text{cm}^{-2}$ ), the final viscoelastic response (figure 2 (c)-(d)) and structure (figure 4(d)) can be varied by a factor of 2.5, which is comparable, for example, to reported changes in the mechanical response of protein hydrogels from metal chelation strategies.<sup>9</sup> As such we propose that they may be utilised as a complementary, and arguably more versatile physical tool that can be used in combination with biochemical approaches to enable a more precise control over viscoelasticity and structure. In future work, we intend to investigate methods to control and quantify the crosslink efficiency and also explore further optimisation of folded protein hydrogel structure and viscoelastic response. Recent simulations from our group have shown that the diffusion timescales, as governed by the protein volume fraction, and the physical properties of the protein monomer are key parameters for tuning hydrogel mechanics.<sup>72</sup> These principles, and those identified in the present work can be utilised together with other tools such as assembly under applied shear,<sup>73</sup> the introduction of complementary non-covalent crosslinking motifs<sup>11</sup> or the modification of the aspect ratio of the constituent folded protein by using chains of covalently conjoined folded protein domains.

## Acknowledgement

This work was funded by the Engineering and Physical Sciences Research Council with grant EP/P02288X/1. The CD spectropolarimeter was funded by the Wellcome Trust with grant WT094232. The authors thank Keith Dredge and Phillip Thornton, University of Leeds for the design and construction of the in-situ illumination devices used in this study and Dr Arwen Tyler, University of Leeds for use of the Anton Parr SAXSpace system and to the

ISIS neutron and muon source for access to the Materials Characterisation Laboratory and the Nano-inXider SAXS.

## Supporting Information Available

Design of in-situ photo-activation rheology device with calibration curves, SAXS spectra and analysis of pre-gel BSA solutions, oscillatory rheology time-sweep data during crosslinking, output parameters of fractal model fitting to BSA hydrogels, pre- and post- gel CD spectra of BSA hydrogels assembled at different rates, examples of constitutive models fitted to creep data.

## References

- (1) Li, Y.; Xue, B.; Cao, Y. 100th Anniversary of Macromolecular Science Viewpoint: Synthetic Protein Hydrogels. *ACS Macro Lett.* **2020**, *9*, 512–524.
- (2) Wheeldon, I. R.; Calabrese Barton, S.; Banta, S. Bioactive proteinaceous hydrogels from designed bifunctional building blocks. *Biomacromolecules* **2007**, *8*, 2990–2994.
- (3) Lv, S.; Dudek, D. M.; Cao, Y.; Balamurali, M.; Gosline, J.; Li, H. Designed biomaterials to mimic the mechanical properties of muscles. *Nature (London)* **2010**, *465*, 69.
- (4) Lv, S.; Cao, Y.; Li, H. Tandem modular protein-based hydrogels constructed using a novel two-component approach. *Langmuir* **2011**, *28*, 2269–2274.
- (5) Lv, S.; Bu, T.; Kayser, J.; Bausch, A.; Li, H. Towards constructing extracellular matrix-mimetic hydrogels: an elastic hydrogel constructed from tandem modular proteins containing tenascin FnIII domains. *Acta Biomater.* **2013**, *9*, 6481–6491.
- (6) Fu, L.; Haage, A.; Kong, N.; Tanentzapf, G.; Li, H. Dynamic protein hydrogels with

- reversibly tunable stiffness regulate human lung fibroblast spreading reversibly. *Chem. Commun. (Cambridge, U. K.)* **2019**, *55*, 5235–5238.
- (7) Kong, N.; Peng, Q.; Li, H. Rationally designed dynamic protein hydrogels with reversibly tunable mechanical properties. *Adv. Funct. Mater.* **2014**, *24*, 7310–7317.
- (8) Khoury, L. R.; Popa, I. Chemical unfolding of protein domains induces shape change in programmed protein hydrogels. *Nat. Commun.* **2019**, *10*, 1–9.
- (9) Kong, N.; Fu, L.; Peng, Q.; Li, H. Metal Chelation Dynamically Regulates the Mechanical Properties of Engineered Protein Hydrogels. *ACS Biomater. Sci. Eng.* **2016**, *3*, 742–749.
- (10) Shmilovich, K.; Popa, I. Modeling protein-based hydrogels under force. *Phys. Rev. Lett.* **2018**, *121*, 168101.
- (11) Wu, J.; Li, P.; Dong, C.; Jiang, H.; Xue, B.; Gao, X.; Qin, M.; Wang, W.; Chen, B.; Cao, Y. Rationally designed synthetic protein hydrogels with predictable mechanical properties. *Nat. Commun.* **2018**, *9*, 620.
- (12) Wang, R.; Li, J.; Li, X.; Guo, J.; Liu, J.; Li, H. Engineering protein polymers of ultrahigh molecular weight via supramolecular polymerization: towards mimicking the giant muscle protein titin. *Chem. Sci.* **2019**, *10*, 9277–9284.
- (13) Hoffmann, T.; Dougan, L. Single molecule force spectroscopy using polyproteins. *Chem. Soc. Rev.* **2012**, *41*, 4781–4796.
- (14) Higham, A. K.; Bonino, C. A.; Raghavan, S. R.; Khan, S. A. Photo-activated ionic gelation of alginate hydrogel: real-time rheological monitoring of the two-step crosslinking mechanism. *Soft Matter* **2014**, *10*, 4990–5002.
- (15) Abete, T.; Del Gado, E.; Serughetti, D. H.; de Arcangelis, L.; Djabourov, M.;

- Coniglio, A. Kinetics of bond formation in cross-linked gelatin gels. *J. Chem. Phys.* **2006**, *125*, 174903.
- (16) Diederich, V. E.; Studer, P.; Kern, A.; Lattuada, M.; Storti, G.; Sharma, R. I.; Snedeker, J. G.; Morbidelli, M. Bioactive polyacrylamide hydrogels with gradients in mechanical stiffness. *Biotechnol. Bioeng.* **2013**, *110*, 1508–1519.
- (17) Burdick, J. A.; Khademhosseini, A.; Langer, R. Fabrication of gradient hydrogels using a microfluidics/photopolymerization process. *Langmuir* **2004**, *20*, 5153–5156.
- (18) Zhu, H.; Yang, X.; Genin, G. M.; Lu, T. J.; Xu, F.; Lin, M. Modeling the mechanics, kinetics, and network evolution of photopolymerized hydrogels. *J. Mech. Phys. Solids* **2020**, 104041.
- (19) Liao, W.; Zhang, Y.; Guan, Y.; Zhu, X. Fractal structures of the hydrogels formed in situ from poly (N-isopropylacrylamide) microgel dispersions. *Langmuir* **2012**, *28*, 10873–10880.
- (20) Poon, W. C.; Haw, M. Mesoscopic structure formation in colloidal aggregation and gelation. *Adv. Colloid Interface Sci.* **1997**, *73*, 71–126.
- (21) Lu, P. J.; Zaccarelli, E.; Ciulla, F.; Schofield, A. B.; Sciortino, F.; Weitz, D. A. Gelation of particles with short-range attraction. *Nature (London)* **2008**, *453*, 499–503.
- (22) Hall, D.; Kardos, J.; Edskes, H.; Carver, J. A.; Goto, Y. A multi-pathway perspective on protein aggregation: implications for control of the rate and extent of amyloid formation. *FEBS Lett.* **2015**, *589*, 672–679.
- (23) Wang, J.; Liu, K.; Xing, R.; Yan, X. Peptide self-assembly: thermodynamics and kinetics. *Chem. Soc. Rev.* **2016**, *45*, 5589–5604.
- (24) Yoshimura, Y.; Lin, Y.; Yagi, H.; Lee, Y.-H.; Kitayama, H.; Sakurai, K.; So, M.; Ogi, H.; Naiki, H.; Goto, Y. Distinguishing crystal-like amyloid fibrils and glass-like amorphous

- aggregates from their kinetics of formation. *Proc. Natl. Acad. Sci. U. S. A.* **2012**, *109*, 14446–14451.
- (25) Fancy, D. A.; Kodadek, T. Chemistry for the analysis of protein–protein interactions: rapid and efficient cross-linking triggered by long wavelength light. *Proc. Natl. Acad. Sci. U. S. A.* **1999**, *96*, 6020–6024.
- (26) Fancy, D. A.; Denison, C.; Kim, K.; Xie, Y.; Holdeman, T.; Amini, F.; Kodadek, T. Scope, limitations and mechanistic aspects of the photo-induced cross-linking of proteins by water-soluble metal complexes. *Chem. Biol. (Oxford, U. K.)* **2000**, *7*, 697–708.
- (27) Lim, K. S.; Klotz, B. J.; Lindberg, G. C.; Melchels, F. P.; Hooper, G. J.; Malda, J.; Gawlitta, D.; Woodfield, T. B. Visible light cross-linking of gelatin hydrogels offers an enhanced cell microenvironment with improved light penetration depth. *Macromol. Biosci.* **2019**, *19*, 1900098.
- (28) Del Gado, E.; Kob, W. Length-scale-dependent relaxation in colloidal gels. *Phys. Rev. Lett.* **2007**, *98*, 028303.
- (29) Winter, H. H.; Chambon, F. Analysis of linear viscoelasticity of a crosslinking polymer at the gel point. *J. Rheol. (Melville, NY, U. S.)* **1986**, *30*, 367–382.
- (30) Muthukumar, M.; Winter, H. H. Fractal dimension of a crosslinking polymer at the gel point. *Macromolecules (Washington, DC, U. S.)* **1986**, *19*, 1284–1285.
- (31) Hsu, S.-h.; Jamieson, A. M. Viscoelastic behaviour at the thermal sol-gel transition of gelatin. *Polymer* **1993**, *34*, 2602–2608.
- (32) Goudoulas, T. B.; Germann, N. Phase transition kinetics and rheology of gelatin-alginate mixtures. *Food Hydrocolloids* **2017**, *66*, 49–60.
- (33) Sarvestani, A. S.; He, X.; Jabbari, E. Viscoelastic characterization and modeling of

- gelation kinetics of injectable in situ cross-linkable poly (lactide-co-ethylene oxide-co-fumarate) hydrogels. *Biomacromolecules* **2007**, *8*, 406–415.
- (34) Takahashi, M.; Yokoyama, K.; Masuda, T.; Takigawa, T. Dynamic viscoelasticity and critical exponents in sol-gel transition of an end-linking polymer. *J. Chem. Phys.* **1994**, *101*, 798–804.
- (35) Ferrone, F. A.; Hofrichter, J.; Sunshine, H. R.; Eaton, W. A. Kinetic studies on photolysis-induced gelation of sickle cell hemoglobin suggest a new mechanism. *Biophys. J.* **1980**, *32*, 361–380.
- (36) Heinson, W.; Chakrabarti, A.; Sorensen, C. M. Kinetic percolation. *Phys. Rev. E* **2017**, *95*, 052109.
- (37) Lin, M.; Lindsay, H.; Weitz, D.; Ball, R.; Klein, R.; Meakin, P. Universality in colloid aggregation. *Nature (London)* **1989**, *339*, 360–362.
- (38) Weitz, D.; Huang, J.; Lin, M.; Sung, J. Limits of the fractal dimension for irreversible kinetic aggregation of gold colloids. *Phys. Rev. Lett.* **1985**, *54*, 1416.
- (39) Poon, W. C. Phase separation, aggregation and gelation in colloid-polymer mixtures and related systems. *Curr. Opin. Colloid Interface Sci.* **1998**, *3*, 593–599.
- (40) Lazzari, S.; Lattuada, M. Growth and Aggregation Regulate Clusters Structural Properties and Gel Time. *J. Phys. Chem. B* **2017**, *121*, 2511–2524.
- (41) Haw, M.; Poon, W. C.; Pusey, P. Structure factors from cluster-cluster aggregation simulation at high concentration. *Phys. A (Amsterdam, Neth.)* **1994**, *208*, 8–17.
- (42) Poling-Skutvik, R.; Lee, J.; Narayanan, S.; Krishnamoorti, R.; Conrad, J. C. Tunable assembly of gold nanorods in polymer solutions to generate controlled nanostructured materials. *ACS Applied Nano Materials* **2018**, *1*, 877–885.

- (43) Hasmy, A.; Anglaret, E.; Foret, M.; Pelous, J.; Jullien, R. Small-angle neutron scattering investigation of long-range correlations in silica aerogels: Simulations and experiments. *Phys. Rev. B* **1994**, *50*, 6006.
- (44) Jachimska, B.; Wasilewska, M.; Adamczyk, Z. Characterization of globular protein solutions by dynamic light scattering, electrophoretic mobility, and viscosity measurements. *Langmuir* **2008**, *24*, 6866–6872.
- (45) Elvin, C. M.; Carr, A. G.; Huson, M. G.; Maxwell, J. M.; Pearson, R. D.; Vuocolo, T.; Liyou, N. E.; Wong, D. C.; Merritt, D. J.; Dixon, N. E. Synthesis and properties of crosslinked recombinant pro-resilin. *Nature (London)* **2005**, *437*, 999.
- (46) Hughes, M. D. G.; Cussons, S.; Mahmoudi, N.; Brockwell, D. J.; Dougan, L. Single molecule protein stabilisation translates to macromolecular mechanics of a protein network. *Soft Matter* **2020**, *16*, 6389–6399.
- (47) Teixeira, J. Small-angle scattering by fractal systems. *J. Appl. Crystallogr.* **1988**, *21*, 781–785.
- (48) Chambon, F.; Winter, H. H. Linear viscoelasticity at the gel point of a crosslinking PDMS with imbalanced stoichiometry. *J. Rheol. (Melville, NY, U. S.)* **1987**, *31*, 683–697.
- (49) Oosawa, F.; Asakura, S.; Hotta, K.; Imai, N.; Ooi, T. G-F transformation of actin as a fibrous condensation. *J. Polym. Sci. (Hoboken, NJ, U. S.)* **1959**, *37*, 323–336.
- (50) Bishop, M. F.; Ferrone, F. A. Kinetics of nucleation-controlled polymerization. A perturbation treatment for use with a secondary pathway. *Biophys. J.* **1984**, *46*, 631–644.
- (51) Ferrone, F. A.; Hofrichter, J.; Eaton, W. A. Kinetics of sickle hemoglobin polymerization: II. A double nucleation mechanism. *J. Mol. Biol.* **1985**, *183*, 611–631.

- (52) Auer, S.; Kashchiev, D. Insight into the correlation between lag time and aggregation rate in the kinetics of protein aggregation. *Proteins: Struct., Funct., Bioinf.* **2010**, *78*, 2412–2416.
- (53) Farrell, S.; DiGuseppi, D.; Alvarez, N.; Schweitzer-Stenner, R. The interplay of aggregation, fibrillization and gelation of an unexpected low molecular weight gelator: glycyllalanyl-glycine in ethanol/water. *Soft Matter* **2016**, *12*, 6096–6110.
- (54) Eden, K.; Morris, R.; Gillam, J.; MacPhee, C. E.; Allen, R. J. Competition between primary nucleation and autocatalysis in amyloid fibril self-assembly. *Biophys. J.* **2015**, *108*, 632–643.
- (55) Knowles, T. P.; Waudby, C. A.; Devlin, G. L.; Cohen, S. I.; Aguzzi, A.; Vendruscolo, M.; Terentjev, E. M.; Welland, M. E.; Dobson, C. M. An analytical solution to the kinetics of breakable filament assembly. *Science (Washington, DC, U. S.)* **2009**, *326*, 1533–1537.
- (56) Cohen, S. I.; Vendruscolo, M.; Welland, M. E.; Dobson, C. M.; Terentjev, E. M.; Knowles, T. P. Nucleated polymerization with secondary pathways. I. Time evolution of the principal moments. *J. Chem. Phys.* **2011**, *135*, 08B615.
- (57) Cohen, S. I.; Vendruscolo, M.; Dobson, C. M.; Knowles, T. P. Nucleated polymerization with secondary pathways. II. Determination of self-consistent solutions to growth processes described by non-linear master equations. *J. Chem. Phys.* **2011**, *135*, 08B611.
- (58) Kuznetsova, I.; Turoverov, K.; Uversky, V. What macromolecular crowding can do to a protein. *Int. J. Mol. Sci.* **2014**, *15*, 23090–23140.
- (59) Ball, R.; Weitz, D.; Witten, T.; Leyvraz, F. Universal kinetics in reaction-limited aggregation. *Phys. Rev. Lett.* **1987**, *58*, 274.
- (60) Loizou, E.; Butler, P.; Porcar, L.; Kesselman, E.; Talmon, Y.; Dundigalla, A.;

- Schmidt, G. Large scale structures in nanocomposite hydrogels. *Macromolecules (Washington, DC, U. S.)* **2005**, *38*, 2047–2049.
- (61) Wu, H.; Xie, J.; Lattuada, M.; Morbidelli, M. Scattering structure factor of colloidal gels characterized by static light scattering, small-angle light scattering, and small-angle neutron scattering measurements. *Langmuir* **2005**, *21*, 3291–3295.
- (62) Meakin, P.; Family, F. Structure and kinetics of reaction-limited aggregation. *Phys. Rev. A* **1988**, *38*, 2110.
- (63) Muthukumar, M. Mean-field theory for diffusion-limited cluster formation. *Phys. Rev. Lett.* **1983**, *50*, 839.
- (64) Jullien, R.; Kolb, M. Hierarchical model for chemically limited cluster-cluster aggregation. *J. Phys. A* **1984**, *17*, L639.
- (65) Flory, P. J. *Principles of polymer chemistry*; Cornell University Press, 1953.
- (66) Bremer, L. G.; van Vliet, T.; Walstra, P. Theoretical and experimental study of the fractal nature of the structure of casein gels. *J. Chem. Soc., Faraday Trans. 1* **1989**, *85*, 3359–3372.
- (67) Van Vliet, T. *Hydrocolloids*; Elsevier, 2000; pp 367–377.
- (68) Landau, L.; Lifshitz, E.; Sykes, J.; Reid, W. *Theory of Elasticity: Vol. 7 of Course of Theoretical Physics*; 1995; Vol. 13.
- (69) Lemaître, A.; Maloney, C. Sum rules for the quasi-static and visco-elastic response of disordered solids at zero temperature. *J. Stat. Phys.* **2006**, *123*, 415.
- (70) DiDonna, B.; Lubensky, T. Nonaffine correlations in random elastic media. *Phys. Rev. E* **2005**, *72*, 066619.

- (71) Basu, A.; Wen, Q.; Mao, X.; Lubensky, T.; Janmey, P. A.; Yodh, A. Nonaffine displacements in flexible polymer networks. *Macromolecules (Washington, DC, U. S.)* **2011**, *44*, 1671–1679.
- (72) Hanson, B. S.; Dougan, L. Network Growth and Structural Characteristics of Globular Protein Hydrogels. *Macromolecules (Washington, DC, U. S.)* **2020**, **In Press**, doi: **10.1021/acs.macromol.0c00890**,
- (73) Whitaker, K. A.; Varga, Z.; Hsiao, L. C.; Solomon, M. J.; Swan, J. W.; Furst, E. M. Colloidal gel elasticity arises from the packing of locally glassy clusters. *Nat. Commun.* **2019**, *10*, 1–8.

# Graphical TOC Entry

